

Exclusive Lepton Pair Production at the Electron-Ion Collider – A Powerful Research Tool

Janusz J. Chwastowski^a, Krzysztof Piotrkowski^b
and Mariusz Przybycien^b *

^a The Henryk Niewodniczański Institute of Nuclear Physics,
Radzikowskiego 152, 31-342 Kraków, Poland

^b AGH University of Science and Technology,
Faculty of Physics and Applied Computer Science,
al. A. Mickiewicza 30, 30-059 Kraków, Poland

September 12, 2022

Abstract

The two-photon exclusive production of lepton pairs at the Electron-Ion Collider will open interesting research directions thanks to a very high luminosity and clean experimental conditions. A survey of the scientific potential of such studies is reported. In particular, we consider unique measurements of the proton elastic electromagnetic form-factors and a possibility of studying the anomalous electromagnetic dipole moments of τ leptons.

Keywords: Two-photon interactions, exclusive production of lepton pairs, proton and ion electromagnetic form-factors, tau leptons, Electron-Ion Collider, EIC.

1 Introduction

The future Electron-Ion Collider and its experiment(s) will provide perfect conditions for studying exclusive processes: (a) a very high luminosity will ensure high statistics data even for relatively rare processes, (b) the data streaming will result in no trigger losses and in a lack of the efficiency corrections, (c) negligible event pileup, excellent particle momentum resolutions and the particle identification (at low and medium transverse momenta) will strongly enhance full final state reconstruction [1]. In addition, in the far-forward and far-backward directions, high resolution detectors of protons and electrons, respectively, will enable the “over-constrained kinematic event reconstruction”, resulting also in possibility of precise data-driven inter-calibrations and tests of the understanding of acceptances and reconstructions.

Thanks to a very high ep luminosity at the EIC, very large samples of exclusively produced lepton pairs can be acquired, opening important research directions – in the following we will mostly discuss the exclusive two-photon production of muon pairs. These first exploratory studies are performed using true kinematic variables, neglecting the detector effects, except from their expected geometrical and kinematic acceptances [1].

2 Monte Carlo event generation and detector acceptance

GRAPE [2] is a Monte Carlo event generator for lepton pair production in electron-proton collisions. The considered processes of di-lepton creation are $\gamma\gamma$, γZ , ZZ and internal photon conversions. Also, effects of

*Corresponding authors:

Janusz.Chwastowski@ifj.edu.pl, Krzysztof.Piotrkowski@agh.edu.pl, Mariusz.Przybycien@agh.edu.pl

the on-/off-shell Z boson production are included, as well as those of the Initial and Final State Radiation (ISR/FSR). The cross-section is calculated using the exact matrix elements at the tree level. The non-zero fermion masses are used in the matrix elements and kinematics. It is also possible to select a sub-set of the diagrams in the calculations. The generator includes also the $e^\pm e^\pm$ interference in the e^+e^- channel. The proton kinematics considers three classes of the scattering processes: elastic, quasi-elastic and DIS.

Below only the elastic case is studied where the proton-proton-photon vertex is calculated using the standard formulae exploiting dipole representation of the proton electromagnetic form-factors:

$$G_E(t) = (1 - t/A_0)^{-2}, \quad G_M(t) = \mu_p G_E(t) \quad (1)$$

where t denotes the four-momentum transfer squared at the proton vertex, $A_0 = 0.71 \text{ GeV}^2$ and μ_p is the proton magnetic moment.

The effect of ISR is included in the cross-section calculation using the structure function method described in [3]. FSR is performed by PYTHIA 6.4 [4] using the parton shower method.

The generated events were required to fulfill the following selection:

- 1) $0.5 < E'_e/E_e < 0.9$ and $\pi - \theta_e < 10$ mrad for the scattered electron,
- 2) $x_L < 0.97$ or $p_T^p > 100 \text{ MeV}/c$, and $\theta_p < 13$ mrad for the scattered proton,
- 3) $p_T^\ell > 300 \text{ MeV}/c$ and $|\eta_\ell| < 3.5$ for leptons belonging to a pair,
- 4) photon veto: no photons above 200 MeV within $|\eta| < 4$,

with $x_L = p_z^p/P_p$, where P_p is the proton beam momentum. The first three demands introduce the EIC detector acceptance and constitute a set of standard requirements. The fourth one, removing events with hard FSR, is sometimes imposed to improve the event kinematics reconstruction.

3 Results

In Fig. 1 the differential cross-sections are shown for the muon pairs passing the selections cuts without the photon veto, at the two energy settings of the EIC: EIC 1 (electron beam energy $E_e = 10 \text{ GeV}$ and proton beam energy $E_p = 100 \text{ GeV}$) and EIC 2 ($E_e = 18 \text{ GeV}$ and $E_p = 275 \text{ GeV}$). Visible threshold effects at the low invariant mass $M_{\mu\mu}$ and transverse momentum of a pair, $p_T^{\mu\mu}$, are due to requirements on the minimal muon p_T^μ and the acceptance of the scattered proton, respectively. The observed total cross-sections are equal to 169 pb and 192 pb (163 pb and 185 pb if the photon veto is applied) for low and high energy beams, respectively. This shows that, given very high luminosities expected at the EIC, the available statistics of exclusive lepton pairs will be very large, even when the full final state is detected.

One should note that clean samples of exclusive muon pairs were collected not only at HERA but also in very harsh conditions at the LHC. The cosmic ray muons can be very efficiently suppressed by tight vertex and acolinearity cuts. In addition, the planned technique of data streaming at the EIC will remove sensitivities to the trigger algorithms as well as maximize the muon acceptance.

3.1 Calibration of far-forward and far-backward detectors

The exclusive muon (and electron) pairs can be used as a powerful tool for calibrating the far-forward and far-backward detectors at the EIC. In Figure 2 the two-dimensional distributions of the muon pair transverse momentum $p_T^{\mu\mu}$ and the proton transverse momentum p_T^p demonstrate a very strong linear correlation, amplified by the requirement of the scattered electron within acceptance of the far-backward detectors, as that ensures a very small p_T transfer at the electron vertex (or, equivalently, a very low photon virtuality Q^2). The longitudinal momenta of the scattered electrons and protons can be calibrated following the Drell-Yan technique used for determination of the fractional momenta of collinear partons from the invariant mass and rapidity of lepton pairs:

$$x_{1,2} = \frac{M_{\ell\ell}}{\sqrt{s}} \sqrt{\frac{(E^{\ell\ell} \pm p_z^{\ell\ell})}{(E^{\ell\ell} \mp p_z^{\ell\ell})}} \exp(\mp Y^*),$$

where x_1, x_2 are the fractional longitudinal momenta transfers at the electron and proton vertices, respectively, $E^{\ell\ell}$ and $p_z^{\ell\ell}$ are the lepton pair energy and longitudinal momentum, and

$$Y^* = \text{arctanh} \left(\frac{P_{e,z} + P_{p,z}}{E_e + E_p} \right)$$

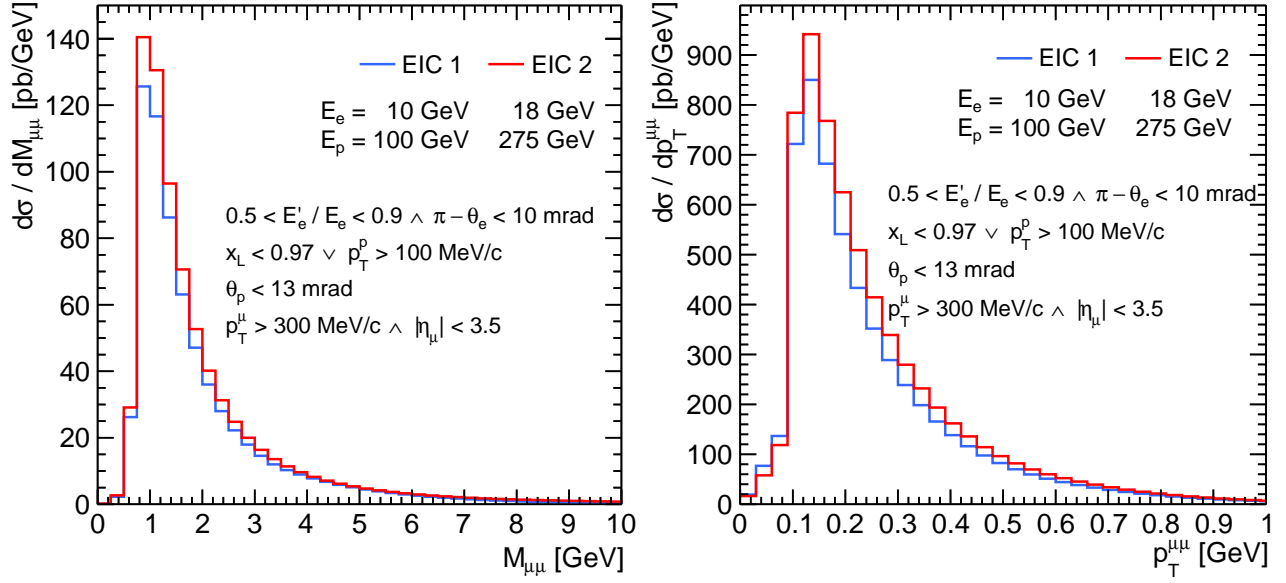


Figure 1: (a) The “observed” cross-section as a function of the invariant mass $M_{\mu\mu}$ for the selected events according to the set of cuts 2, without the photon veto, for the high (red histogram) and low (blue histogram) energy collisions at the EIC; (b) the corresponding cross-sections for the muon pair as a function of $p_T^{\mu\mu}$.

is the rapidity of the centre-of-mass reference frame.

In Fig. 3 the “reconstructed” x_1, x_2 are compared to $1 - x_L$ and $1 - E'_e/E_e$. The photon veto was applied to minimize the FSR impact, as well as the cut on the muon pair, $p_T^{\mu\mu} < 200$ MeV/c, to maximize collinearity of the exchanged photons. The obtained distributions are narrow with the FWHM below 1%, and a sharp kinematic cut-off.

Given a large statistics of the selected sample and a high resolution of reconstruction of the muons by the central detectors, this will result in a possibility of regular precise calibrations of the far-forward and far-backward detectors. In addition, the exclusive electron-positron pairs will nearly double the statistics of such unique calibration samples. Moreover, as the detection of the forward-scattered proton ensures the exclusivity of the event, one can lift the requirement of the detection of scattered electron and use such an “untagged” sample to determine the acceptance of the far-backward detectors directly from the experimental data.

3.2 Sensitivity to the proton charge radius

There are observed continuing discrepancies among measurements of the proton charge radius R_p , in particular among “classical” measurements using electron-proton elastic scattering [5, 6] (see also [7] for discussion of the experimental results). Precise measurements of the exclusive production of lepton pairs at the EIC may help to sort out this puzzle. Below, we investigate the ultimate statistical precision of the R_p determination at the EIC.

The mean proton charge radius R_p can be obtained from the proton electric form-factor using the following relation:

$$R_p^2 = 6 \left[\frac{1}{G_E} \frac{dG_E}{dt} \right]_{t=0}, \quad (3)$$

hence, $R_p^2 = 12/0.71$ GeV² for the “standard” dipole G_E . Therefore, for the dipole form-factors, the change of the nominal parameter $A_0 = 0.71$ GeV² (Eq. (1)) is equivalent to the corresponding change of the nominal value of the proton radius $R_p = 0.811$ fm.

To evaluate the statistical sensitivity to R_p two ratios of the “observed” differential cross-sections in t were calculated using three different values of the A parameter in the dipole form-factors, or equivalently for three values of R_p . As the elastic cross-sections for the exclusive lepton pairs calculated by GRAPE are

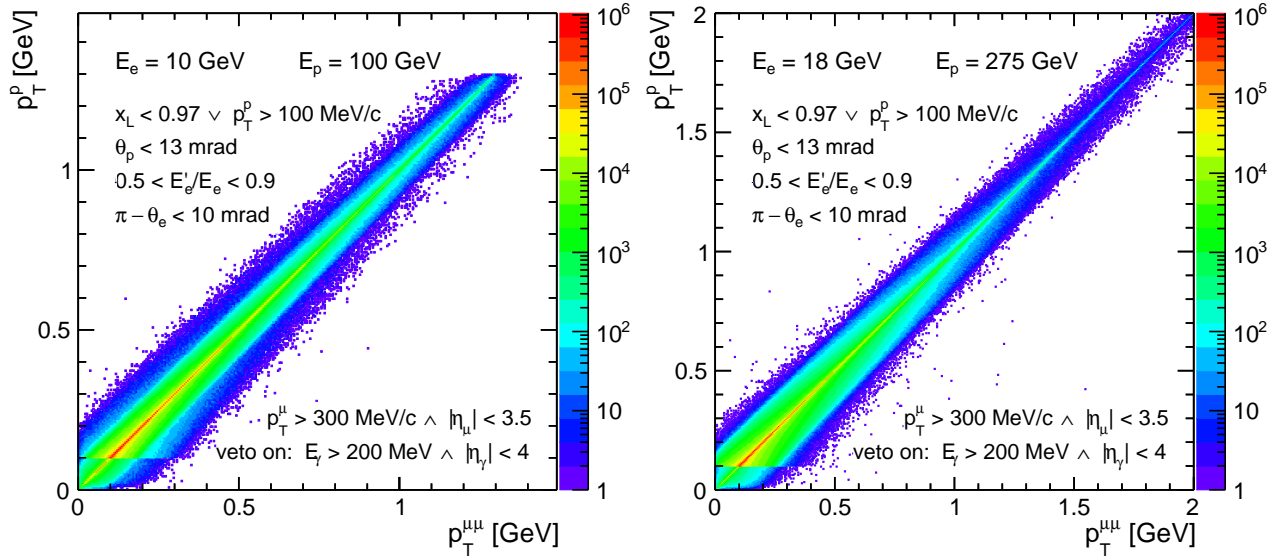


Figure 2: Correlation of the lepton pair transverse momentum, $p_T^{\mu\mu}$, and the proton transverse momentum, p_T^p for two energy configurations of the EIC. The photon veto (2.4) was applied.

proportional to G_E^2 , therefore, close to $t = 0$, their ratios are directly sensitive to the proton charge radius:

$$\left. \frac{d}{dt} \left(\frac{d\sigma}{dt}(A_1) / \frac{d\sigma}{dt}(A_2) \right) \right|_{t=0} = \frac{1}{3}(R_1^2 - R_2^2). \quad (4)$$

Figure 4 shows the ratios of the observed cross-sections – $d\sigma/dt$ obtained with $A = 0.69 \text{ GeV}^2$ or 0.73 GeV^2 , to the “standard” one for $A = A_0$. The expected derivatives at $t = 0$ are equal, according to Eq. 4, to 0.163 and -0.154 for $A_1 = 0.69 \text{ GeV}^2$ and 0.73 GeV^2 , respectively, and $A_2 = A_0$. One should note that in order to increase the observed cross-sections and to avoid sensitivity to the bremsstrahlung overlays in the far-backward detectors the detection of the scattered electron was not required.

The fitted slopes in the $|t|$ -range of $0 - 0.05 \text{ GeV}^2$ agree well with the above expectations (the fitted slopes have the opposite sign to the corresponding derivatives) and the associated statistical uncertainties provide estimates of ultimate sensitivities to R_p . The simulated data samples correspond to the EIC integrated luminosity of about 100 fb^{-1} and the estimated statistical uncertainty on R_p is very small, of about 0.1%.

The impact of the proton beam angular divergence and its energy dispersion was checked by “smearing” the proton momenta according to the EIC beam parameters [8]. Fits to the smeared t -distributions resulted in new slopes only weakly changed, within statistical errors of the results reported in Fig. 4.

Resolutions of far-forward detectors will introduce additional event “migrations” and smearing of t -distributions – corrections for these effects, including the proton beam divergence, will result in systematic uncertainties. Such problems will be addressed in future publications; here the ultimate potential for such measurements is discussed. One should note that the total integrated luminosity of the order of 1000 fb^{-1} is expected at the EIC, and in addition the exclusive electron-positron pairs can also be used for such studies. That will lead to yet much bigger data samples, taken at various beam energies and polarizations, allowing for many powerful studies of potential systematic effects.

The above demonstrates that the measurements of exclusive lepton pairs at the EIC may enable unique determinations of the proton charge radius with competitive precision. The proposed technique can also be applied to perform novel measurements of the elastic form-factors and charge radii of light ions, such as the deuterium and helium nuclei, for which the far-forward detectors at the EIC will still have significant acceptances and for which the experimental data show some tension [9, 10].

In the case of heavy nuclei, as the gold nuclei, the elastically scattered ions cannot be detected, therefore the t -dependence of the cross-section will be measured using the transverse momentum of the lepton pair. In this case, the tagging of low- Q^2 events using the far-backward detectors might be mandatory to get the best t resolution. The major systematic problem will appear, however, because of the contribution of non-elastic

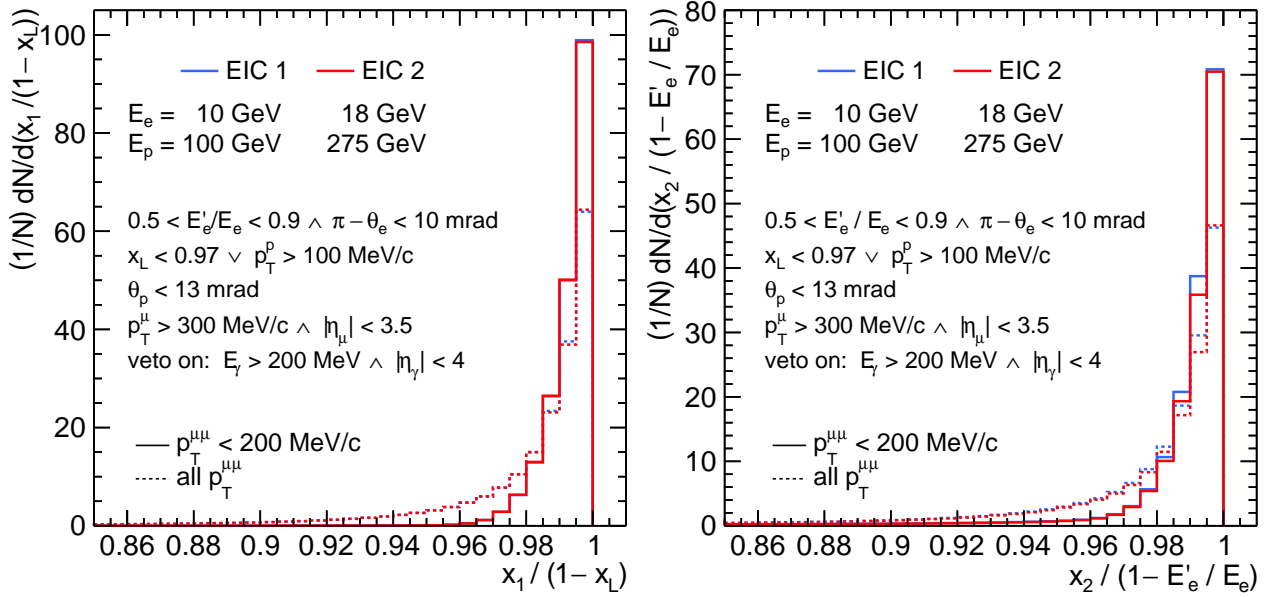


Figure 3: Distributions of $x_1/(1-x_L)$ and $x_2/(1-E'_e/E_e)$ with (solid line) and without (dotted line) the cut on the transverse momentum of the lepton pair $p_T^{\mu\mu} < 200$ MeV/c.

(or semi-exclusive) events, when an incident ion gets excited or dissociates into a system of a larger mass, as a result of an interaction.

3.3 Electromagnetic form-factors at higher photon virtualities

Precise measurements of the proton electromagnetic form-factors are also of interest at larger $|t|$, at 1 GeV² and beyond, where the perturbative calculations can be performed. These two elastic form-factors are contained in the Generalized Parton Distributions (GPDs) (see for example [11]). However, the GPDs cannot yet be determined fully from first principles the high precision data will deliver an experimental platform for further constraining of them, cf. [12] or can be used to discuss the lattice QCD predictions, e.g. [13].

In Fig. 5, the observed $|t| \cdot d\sigma/d|t|$ distributions are shown for electron-proton scattering, demonstrating the large $|t|$ reach also at low energy EIC running. At high energies a significant cross-section is expected even at $|t| \approx 4$ GeV². One should note that also here the requirement of electron detection could be lifted, leading to a large increase of the observed cross-section and to a lack of sensitivity to the bremsstrahlung overlays in the far-backward detectors. At such a high $|t|$, the G_M contribution dominates but the G_E one is still significant allowing their separation by combining data at different beam energies. Moreover, the high polarization of incident protons will enable construction of the azimuthal $p - \mu\mu$ correlations, for example, to enhance the separation power of the G_E and G_M contributions.

As in the case of the proton charge radius, the EIC ion beams will allow us to extend such a studies by supplementing them with unique investigations of the nuclear effects. It is particularly exciting for the light ion beams for which a high polarization will be available [8].

3.4 The exclusive pairs of tau leptons

Exclusive production of τ pairs via photon-photon fusion in the Ultra Peripheral Collisions (UPC) of heavy ions has recently become a vigorous research activity [14]. It was shown that such a two-photon pair production is particularly sensitive to the anomalous electromagnetic dipole moments of τ leptons. Here we evaluate the EIC scientific potential in this domain.

In Fig. 6 the differential cross-sections in the invariant mass $M_{\tau\tau}$ are shown for the $\tau^+\tau^-$ pairs of the accepted events (without imposing the photon veto). The corresponding total observed cross-sections are: $\sigma_{\text{obs}}^{\tau\tau}(\text{EIC 1}) = 5.5$ pb and $\sigma_{\text{obs}}^{\tau\tau}(\text{EIC 2}) = 7.8$ pb. These cross-sections are large in spite of requiring the detection of the scattered electron and proton, to ensure the best reconstruction of the event kinematics. As

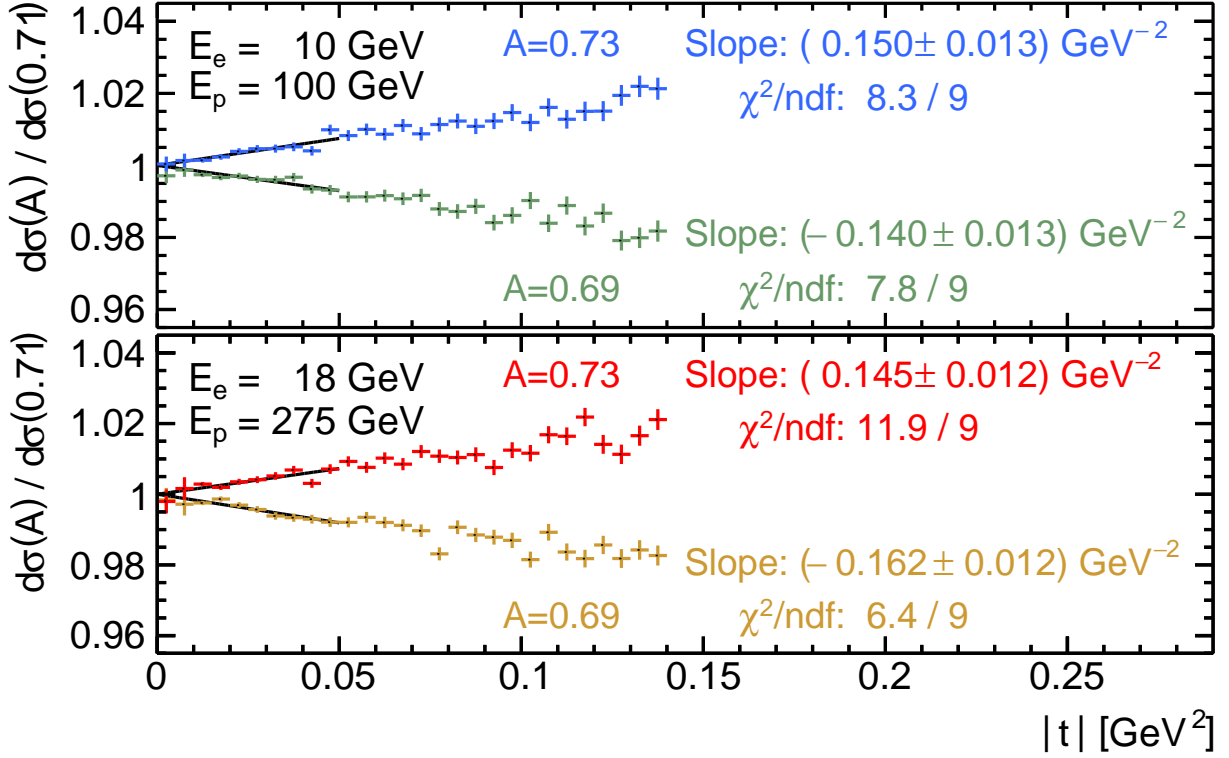


Figure 4: Ratios of the observed cross-sections $d\sigma/dt$ for $A = 0.69 \text{ GeV}^2$ and 0.73 GeV^2 with respect to the “standard” $d\sigma/dt(A_0)$; statistical errors correspond to the integrated luminosity of 106 and 99 fb^{-1} for low (upper plot) and high (lower plot) energy beams, respectively. The fitted slopes at $t \approx 0$ are also displayed. Neither electron requirement nor the photon veto were imposed (only cuts 2.2–3 were applied).

a result, the expected $\tau^+\tau^-$ event samples at the EIC are very large – about two orders of magnitude bigger than those expected to be collected at the High Luminosity Large Hadron Collider (HL-LHC) [15]. One should note that in Fig. 6 the detection of all τ leptons produced within “geometrical acceptance” of the EIC central detectors is assumed. In contrast to the UPC case, this should not be far from reality given the lack of trigger inefficiencies at the EIC, thanks to the data streaming, and the central detectors optimized for low and medium p_T particle reconstruction and identification.

The detection of the scattered electron might not be necessary, in which case the event statistics will increase by an order of magnitude. Such experimental issues will be further studied, as well as the use of the proton beam polarization to amplify the sensitivity to the the anomalous electromagnetic dipole moments of τ leptons at the EIC.

4 Conclusions and outlook

The first exploratory survey of the exclusive lepton pair production at the EIC reveals excellent prospects for studying such processes. The combination of very high luminosities, very hermetic high resolution detectors, clean experimental environment, high beam polarisations and large variety of ion beams provides ideal conditions for further investigations.

The exclusive lepton pairs at the EIC are a powerful tool offering profound insights into the structure of hadrons as well as unique studies of the τ lepton properties.

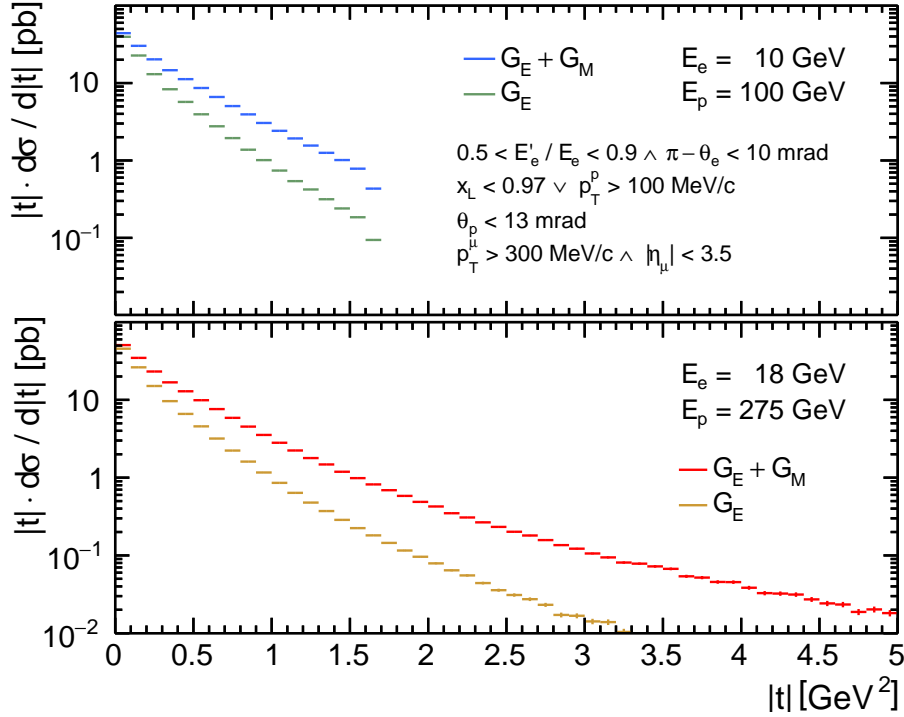


Figure 5: Differential cross-sections, $|t| \cdot d\sigma/d|t|$, for accepted the events without the photon veto; for low (upper) and high (lower) energy beams, where the statistical errors correspond to the integrated luminosity of about 300 fb^{-1} . The plots compare distributions obtained using the full form-factor and those for which the magnetic form-factor was switched off.

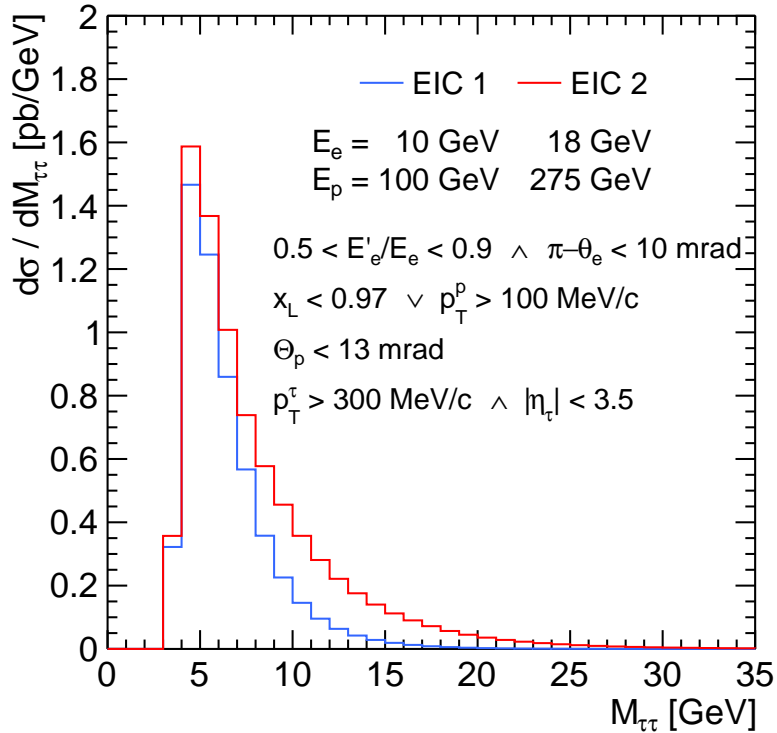


Figure 6: The differential cross-section in the invariant mass $M_{\tau\tau}$ of selected events according to “acceptance cuts” (see Sec. 2, without photon veto) for electron proton collisions at high (red histogram) and low (blue histogram) beam energies.

References

- [1] R. Abdul Khalek et al. Science Requirements and Detector Concepts for the Electron-Ion Collider: EIC Yellow Report., 3 2021. [arXiv:2103.05419](#).
- [2] Tetsuo Abe. GRAPE dilepton (Version1.1): A Generator for dilepton production in ep collisions. *Comput. Phys. Commun.*, 136:126–147, 2001. [arXiv:hep-ph/0012029](#), [doi:10.1016/S0010-4655\(00\)00246-0](#).
- [3] J. Fujimoto, M. Igarashi, N. Nakazawa, Y. Shimizu, and K. Tobimatsu. Radiative corrections to e^+e^- reactions in electroweak theory. *Prog. Theor. Phys. Suppl.*, 100:1–379, 1990. [doi:10.1143/PTPS.100.1](#).
- [4] Torbjorn Sjostrand, Stephen Mrenna, and Peter Z. Skands. PYTHIA 6.4 Physics and Manual. *JHEP*, 05:026, 2006. [arXiv:hep-ph/0603175](#), [doi:10.1088/1126-6708/2006/05/026](#).
- [5] J. C. Bernauer et al. Electric and magnetic form factors of the proton. *Phys. Rev. C*, 90(1):015206, 2014. [arXiv:1307.6227](#), [doi:10.1103/PhysRevC.90.015206](#).
- [6] W. Xiong et al. A small proton charge radius from an electron–proton scattering experiment. *Nature*, 575(7781):147–150, 2019. [doi:10.1038/s41586-019-1721-2](#).
- [7] Simone Pacetti and Egle Tomasi-Gustafsson. The origin of the proton radius puzzle. *Eur. Phys. J. A*, 57(2):72, 2021. [doi:10.1140/epja/s10050-021-00398-8](#).
- [8] Ferdinand Willeke. Electron Ion Collider Conceptual Design Report 2021. 2 2021. [doi:10.2172/1765663](#).
- [9] Randolph Pohl et al. Laser Spectroscopy of Muonic Atoms and Ions. *JPS Conf. Proc.*, 18:011021, 2017. [arXiv:1609.03440](#), [doi:10.7566/JSPSC.18.011021](#).
- [10] O.J. Hernandez, A. Ekström, N. Nevo Dinur, C. Ji, S. Bacca, and N. Barnea. The deuteron-radius puzzle is alive: A new analysis of nuclear structure uncertainties. *Physics Letters B*, 778:377–383, 2018. URL: <https://www.sciencedirect.com/science/article/pii/S0370269318300510>, [doi:https://doi.org/10.1016/j.physletb.2018.01.043](#).
- [11] A. V. Belitsky and A. V. Radyushkin. Unraveling hadron structure with generalized parton distributions. *Phys. Rept.*, 418:1–387, 2005. [arXiv:hep-ph/0504030](#), [doi:10.1016/j.physrep.2005.06.002](#).
- [12] M. Diehl, Th. Feldmann, R. Jakob, and P. Kroll. Generalized parton distributions from nucleon form-factor data. *Eur. Phys. J. C*, 39:1–39, 2005. [arXiv:hep-ph/0408173](#), [doi:10.1140/epjc/s2004-02063-4](#).
- [13] C. Alexandrou, S. Bacchio, M. Constantinou, J. Finkenrath, K. Hadjiyiannakou, K. Jansen, G. Koutsou, and A. Vaquero Aviles-Casco. Proton and neutron electromagnetic form factors from lattice QCD. *Phys. Rev. D*, 100(1):014509, 2019. [arXiv:1812.10311](#), [doi:10.1103/PhysRevD.100.014509](#).
- [14] ATLAS Collaboration. Observation of the $\gamma\gamma \rightarrow \tau\tau$ process in Pb+Pb collisions and constraints on the τ -lepton anomalous magnetic moment with the ATLAS detector. 4 2022. [arXiv:2204.13478](#).
- [15] Mateusz Dyndal, Mariola Klusek-Gawenda, Matthias Schott, and Antoni Szczurek. Anomalous electromagnetic moments of τ lepton in $\gamma\gamma \rightarrow \tau^+\tau^-$ reaction in Pb+Pb collisions at the LHC. *Phys. Lett. B*, 809:135682, 2020. [arXiv:2002.05503](#), [doi:10.1016/j.physletb.2020.135682](#).